NJC

Accepted Manuscript

This is an *Accepted Manuscript*, which has been through the Royal Society of Chemistry peer review process and has been accepted for publication.

Accepted Manuscripts are published online shortly after acceptance, before technical editing, formatting and proof reading. Using this free service, authors can make their results available to the community, in citable form, before we publish the edited article. We will replace this *Accepted Manuscript* with the edited and formatted *Advance Article* as soon as it is available.

You can find more information about *Accepted Manuscripts* in the Information for Authors.

Please note that technical editing may introduce minor changes to the text and/or graphics, which may alter content. The journal's standard Terms & Conditions and the Ethical guidelines still apply. In no event shall the Royal Society of Chemistry be held responsible for any errors or omissions in this *Accepted Manuscript* or any consequences arising from the use of any information it contains.

ROYAL SOCIETY OF CHEMISTRY

www.rsc.org/njc

New Journal of Chemistry RSCPublishing

ARTICLE

Neuron-like polyelectrolyte/carbon nanotube composites for ultra-high loading of metal nanoparticles

Cite this: DOI: 10.1039/x0xx00000x

Received 00th January 2012,
Accepted 00th January 2012

DOI: 10.1039/x0xx00000x

www.rsc.org/

Md. Shahinul Islam,[a] Won San Choi,[b,*] Tae Sung Bae,[a] Young Boo Lee[a] and Ha-Jin Lee[a,c,*]

We report a simple protocol for the fabrication of multiwall carbon nanotubes (MWCNTs) with a neuron-like structure for loading ultra-high densities of metal nanoparticles (NPs). The MWCNTs were initially coated with an anionic polyelectrolyte (PE), polystyrene sodium sulfonate (PSS), using a noncovalent interaction (CNT/PSS). The neuron-like structures were fabricated through the stepwise assembly of both the positively charged poly(allylamine) hydrochloride (PAH) and negatively charged poly(acrylic acid) (PAA) in a nonstoichiometric ratio on the CNT/PSS as a template. After three coatings with the PEs, the obtained neuron-shaped CNTs were used as a support for loading a high density of multi-metallic NPs. Moreover, a unique characteristic, tunable and side specific growth of the metal NPs, was also observed. Our neuron-like structures with high loadings of multi-metallic NPs were demonstrated to be catalytic materials for the conversion of 4-nitrophenol to 4-aminophenol and as a convenient surface-enhanced Raman scattering substrate for biological tags and molecular detection.

I Introduction

Recent advances in nanoparticle (NP) synthetic methodologies have led to the development of well-dispersed, metal-based catalysts, which has become an important frontier of nanomaterial studies. Specially, the synthesis and catalytic uses of mono-, bi-, and multi-metallic alloys or core-shell NPs using a variety of capping/stabilizing agents, such as surfactant micelles, dendrimers, or functional polymers, have drawn considerable attention.[1,2] A central problem of the stabilizing agents is their strong interactions with metal NPs, which may alter the catalytic properties of the NPs. Moreover, the leaching of heavy metals or even dissolution may be another problem for the recovery and reuse of metal NPs.[3,4] On the other hand, embedding metal NPs within polymer/polyelectrolyte matrices for practical applications, such as optoelectronics and sensor devices, show promising potential.[5] Compared to the polymer chain itself, polymeric complexes have an abundance of compositions, relatively large dimensions, and diverse structures, which can be easily tailored by changing the procedure for the formation of polymeric complexes.[6] Among the various types of polymeric matrices, polyelectrolyte complexes (PECs) are of considerable interest because various polyelectrolytes (PEs) are readily available. Moreover, the PECs produced using a simple mixing of oppositely charged PEs can be utilized for a wide range of metal NPs-based applications due to their large surface areas and various functional groups for high loadings of metal NPs.[7-11] Here, the PEC matrix has a dual role: i) to provide a scaffold for immobilizing NPs and preventing their aggregation, and ii) to serve as a capping agent for limiting the growth of metal NPs.[12] However, most of the PECs reported to date have been used as templates. Relatively little attention has been focused on the synthesis of PEC-based nanocomposites using PEC as coating materials rather than as a template. Thus, the use of PECs as coating materials for the preparation of PEC-based nanocomposites with a controllable structure is highly desirable and has considerable potential for future applications.

Carbon nanotubes (CNTs) are the smallest organized form of carbon, and they have received increasing scientific interest due to their unique structural, mechanical and electrical properties, which have made them one of the most attractive candidates for various potential applications.[13] One way to promote the widespread use of CNTs in real applications is to develop a methodology to disperse or solubilize them in solvents. One simple method to disperse CNTs in aqueous media is to wrap them with PEs via layer-by-layer (LBL) self-assembly.[14-17] There is still considerable interest in developing novel wrapping methods for the preparation of CNT/PE-based nanocomposites with hierarchical structures, which exhibit unique characteristics for potential applications.

Here, we employed multiwall carbon nanotubes (MWCNTs) as templates to highly load metal NPs, and we successfully fabricated a metal NP-embedded MWCNT neuron-like structure via an LbL assembly technique using oppositely charged PEs. The as-received MWCNTs (p-CNT) were initially coated with an anionic PE, polystyrene sodium sulfonate (PSS), using noncovalent van der Waals interactions. Then, the coated MWCNTs were used as a template for the chronological

New Journal of Chemistry Accepted Manuscript

assembly of both the positively charged poly(allylamine) hydrochloride (PAH) and negatively charged poly(acrylic acid) (PAA) in a nonstoichiometric ratio. Because the wrapping of PSS along the sidewall of p-CNTs formed discontinuous bumps, the subsequent PEs were limitedly assembled onto certain irregular bumps on the p-CNT/PSS. Therefore, the neuron-shaped hybrid structure of PEs could be formed on the p-CNTs. The obtained necklace CNTs (denoted as CNT/PSS/PAH/PAA) were tested as a support for high loadings of multi-metallic hybrid NPs (Au/Pt, Au/Ag, Ag/Pt, or Au/Pt/Ag/Pd). We also report the use of these metal NP-embedded neuron-like structures for applications that demand enhanced surface-enhanced Raman scattering (SERS) and catalytic activities.

II Experimental section

Materials. Polystyrene sodium sulfonate (PSS, Mw=70,000), poly(allylamine) hydrochloride (PAH, Mw = 15,000), poly(acrylic acid) (PAA, Mw = 1,800), silver nitrate ($AgNO_3$, 99.99%), chloroauric acid (HAuCl4, 99.99%), chloroplatinic acid (H_2PtCl_6, 99.99%), palladium nitrate (PdN_2O_6), sodium borohydride ($NaBH_4$), 4-nitrophenol (4-NPh), and 4-aminothiophenol (4-ATP) were purchased from Sigma-Aldrich. Multiwall carbon nanotubes (MWCNTs, CM-95) were obtained from the Hanwha Nanotech Co. Korea. All chemicals were used without further purification. The PEs and metal precursor solutions were prepared with deionized (DI) water obtained from a Millipore Simplicity 185 system. The pH was adjusted with 0.1 M HNO_3 or 0.1 M NaOH. The concentrations of all metal precursors were maintained at 2.5 mM in elsewhere.

Synthesis of neuron-like structure of MWCNT (p-CNT/PSS/PAH/PAA). Initially, MWCNT (0.2 mg/mL) was ultrasonicated in water/ethanol (1:1) for 1 hour. The desired PSS-coated MWCNTs (denoted as p-CNT/PSS) were prepared by mixing 5 mL of the predispersed p-CNT aqueous solution and 20 mL of a PSS solution (1 mg/mL) under ultrasonic treatment for 2 hours. The resulting p-CNT/PSS was collected by centrifugation at 10,000 rpm and washed with DI water to remove excess PSS. Then, the precipitates were dried and redispersed in water at a concentration of 1 mg/mL. In next step, p-CNT/PSS was used for fabrication of necklace structure using two oppositely charged PEs (PAH and PAA) into nonstoichiometric ratio (1.5:0.60); 5 mL of p-CNT/PSS was mixed with 5 mL of a PAH solution (1.5 mg/mL, pH=7) using ultrasonic treatment for 1 hour. The resulting product was denoted as a p-CNT/PSS/PAH. Finally, 5 mL of a PAA solution (0.60 mg/mL, pH=~4.0) was added to the p-CNT/PSS/PAH and further sonicated for 1 hour. Excess PAH or PAA was removed by centrifuging and successive washing with DI water. The final product was denoted as p-CNT/PSS/PAH/PAA.

Synthesis of multi-metallic NP-CNT/PSS/PAH/PAA (CNT/PSS/PAH/PAA-*M*, where *M* = Au, Pt, Ag, and/or Pd). The route for synthesizing metal NP-embedded CNT/PSS/PAH/PAA was initiated by employing p-CNT/PSS as a template. Before this step, it was necessary to prepare metal precursor-embedded PAH or PAA, *i.e.,* PAH-M_1 (M_1=Au, Pt or Au/Pt) or PAA-M_2, (M_2=Ag, Pd or Ag/Pd). For example, to prepare PAH/Au, the pH value of PAH should be changed to 9.0 to ensure the complete ionization of its amino groups. Then, 1 mL of an aqueous $HAuCl_4$ solution was added into the PAH solution (10 mL, 1.5 mg/mL) and stirred for 1 hour. By following a similar approach, PAH/Pt was prepared using an aqueous H_2PtCl_6 solution (1 mL) instead of a $HAuCl_4$ solution. The details for the synthesis and characterization of mono-metallic NP-embedded PAH and PAA have been described in our previous work.[18] To prepare PAH-Au/Pt, 1 mL of a mixture (1:1=v/v) of the H_2PtCl_6 and $HAuCl_4$ aqueous solutions was used. For PAA-Ag, after adjusting the pH value of the PAA aqueous solution to 5.5, the PAA solution (10 mL, 0.60 mg/mL) was mixed with 1 mL of an aqueous $AgNO_3$ solution and stirred for 1 hour. PAA/Pd was prepared using an aqueous PdN_2O_6 solution (1 mL) instead of an $AgNO_3$ solution. Using a mixture (1:1=v/v) of $AgNO_3$ and PdN_2O_6 aqueous solutions allowed us to prepare PAA-Ag/Pd. Subsequently, the metal precursor-loaded PAH, PAH-M_1 (M_1=Au, Pt or Au/Pt), was mixed with p-CNT/PSS at a 1:1 volume ratio by ultrasonic treatment for 1 hour. The p-CNT/PSS/PAH-M_1 (M_1=Au, Pt or Au/Pt) was collected after centrifuging and washing with DI water 3 times. Finally, according to the experimental requirements, PAA-M_2 (M_2=Ag, Pd or Ag/Pd) was blended with p-CNT/PSS/PAH-M_1 to obtain bi- or tetra-metallic necklace-shaped p-CNT/PSS/PAH/PAA-*M*. Excess metal salts, PAH or PAA were removed using centrifugation and successive washings with DI water. Finally, the metal precursor-embedded CNT/PSS/PAH/PAAs were reduced to metal NP-embedded CNT/PSS/PAH/PAA using $NaBH_4$.

Catalytic testing of p-CNT/PSS/PAH/PAA-*M* for the reduction of 4-NPh and SERS measurements. The catalytic reduction of 4-NPh by $NaBH_4$ in the presence of the CNT/PSS/PAH/PAA-*M* was studied by UV-vis absorption spectroscopy; 1 mL of $NaBH_4$ (10 mM) was mixed with 0.5 mL of 4-NPh (0.5 mM) in a UV quartz cell (1 × 1 cm^2), and 0.15 mL of the CNT/PSS/PAH/PAA-*M* solution was added to the mixture in the cell. The absorption spectra were recorded at constant time intervals in the spectral range of 200–600 nm at room temperature. To measure the SERS of the p-CNT/PSS/PAH/PAA-*M* and 4-ATP, a total of 100 mL of the multi-metallic catalyst solution was dropped onto a glass substrate and dried in air. Then, 50 mL of an ethanol solution containing 0.25 mM 4-ATP was dropped onto the p-CNT/PSS/PAH/PAA-*M*-coated glass substrate. Then, the substrate was dried and washed. Finally, SERS spectra were recorded under a laser beam with an accumulation time of 5 s and 3 mW of laser power with an excitation wavelength of 632.8 nm. For reusability test, after completing the catalytic reaction, the catalyst was separated by centrifugation and reused for further reduction of 4-NPh.

Characterization. The microscopic characterizations of the fabricated samples were conducted using field emission-transmission electron microscopy (FE-TEM) on a JEOL JEM 2100F and using ultrahigh resolution field emission-scanning electron microscopy (UHR-FESEM) on a Hitachi S-5500. X-ray photoelectron spectroscopy (XPS) studies were performed using an Axis NOVA (Kratos analytical) spectrometer with an aluminum anode (Al Kα, 1486.6 eV) operating at 600 W. Raman analyses were performed using a scanning confocal Raman microscope (Nanofinder 30, Tokyo Instruments) with a laser excitation wavelength of 632.8 nm (HeNe laser). ζ-potential measurements were performed on a Malvern Nano-ZS Zetasizer at room temperature using ethanol as a solvent. UV−vis absorption spectra were recorded on a UV-vis-NIR spectrophotometer (Shimadzu UV-3600). Thermal gravimetric analysis (TGA) was performed using a TA Instrument Hi-Res TGA 2950 thermogravimetric analyzer at a heating rate of 5 ^oC/min under air atmosphere.

III Results and Discussion

The preparation strategy for constructing the necklace-structure MWCNTs is shown in Fig. 1a. Pristine MWCNTs (p-CNT) were initially coated with negatively charged PSS using a secondary interaction, such as van der Waals (*i.e.,* p-CNT/PSS).

New Journal of Chemistry Accepted Manuscript

This journal is © The Royal Society of Chemistry 2012

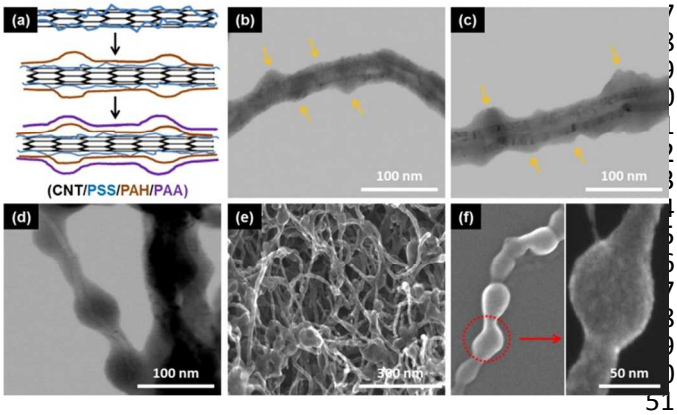

Fig. 1 (a) A schematic representation of the necklace-shaped MWCNTs fabricated by the chronological mixing of anionic and cationic PEs in a nonstoichiometric ratio. Representative TEM images of (b) p-CNT/PSS, (c) p-CNT/PSS/PAH, and (d) p-CNT/PSS/PAH/PAA. Arrows indicate discontinuous bumps consisting of PEs on the p-CNT surface. (e and f) UHR-FESEM images of CNT/PSS/PAH/PAA.

In subsequent steps, negatively charged p-CNT/PSS was employed as a template for the next step, leading to the fabrication of the necklace structure of p-CNT. This step was performed by sequentially coating PAH and PAA onto the p-CNT/PSS templates using a nonstoichiometric volume ratio. The TEM micrographs of p-CNT/PSS show a PSS coating with an irregular thickness on the surfaces of the p-CNTs (Fig. 1b). The zeta potential value of –55.10 mV confirms that the negatively charged PSS was coated on the p-CNTs (Fig. S1a). Subsequently, the zeta potential value changed to a positive value of +32.28 mV due to the primary amine ($-NH_3^+$) groups of PAH, which confirmed coating of cationic PAH onto the anionic p-CNT/PSS templates (Fig. S1b). The obtained semi-necklace structures were denoted as p-CNT/PSS/PAH elsewhere (Fig. 1c). Finally, the p-CNT/PSS/PAH was further coated with anionic PAA, and well-defined necklace structures were obtained (Fig. 1d-f). The zeta potential value was changed to -4.19 mV due to the presence of the carboxylic acid (-COOH) groups of PAA (Fig. S1c). Additional electron micrographs revealed the process of forming neuron-like structures composed of p-CNT and polyelectrolytes (Fig. S2).

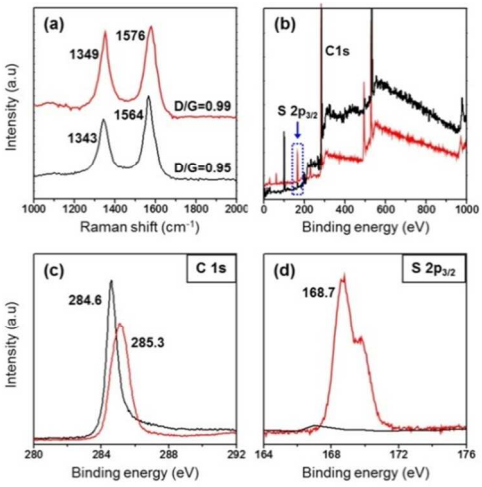

Fig. 2 (a) Raman spectra and (b-d) XPS spectra of p-CNT before (black line) and after (red line) PSS treatment, (b) survey, (c) C 1s core-level, and (d) S 2p core-level .

Raman and XPS data further confirmed the stepwise coating of polyelectrolytes onto p-CNTs. The Raman spectra showed that the D/G ratio of the p-CNTs increased from 0.95 to 0.99 after the coating of PSS onto p-CNTs (Fig. 2a). The increasing intensity of the D-band after the coating of PSS onto the p-CNTs indicates an increasing number of defects on the p-CNT surfaces.[19] Notably, both the D- and G-bands in the p-CNT/PSS were shifted to higher wavenumbers (from 1343 to 1349 cm^{-1} for the D-band and from 1564 to 1576 cm^{-1} for the G-band) compared to the p-CNTs. This behavior means that the defect sites of the p-CNTs interact sensitively with the PSS and results in a debundling of the p-CNTs.[20] The XPS data showed a characteristic peak at 168.7 for $S2p_{3/2}$, which comes from the sulfonate groups of PSS in p-CNT/PSS (Fig. 2b and 2d). Additionally, shifting of the C1s peak of p-CNT from 284.6 eV to 285.3 eV indicates that PSS possessing a C-S moiety was coated on the p-CNTs (Fig. 2c). Additional XPS data confirming the presence of N1S after the coating of PAH onto the p-CNT/PSS can be found in Fig. S3.

It was observed that the PSS did not wrap the p-CNTs in a continuous manner but rather formed discontinuous bumps on the surfaces of the p-CNTs (Fig. 1b). Therefore, when the p-CNT/PSS was employed as a template for additional coating with cationic PAH through electrostatic interactions, some interaction points on the bumps of the p-CNT/PSS can be easily exposed for the next coating. Fig. 1c and S2 clearly show the bumps that grew on the p-CNT/PSS/PAH surface. The positive zeta potential value of p-CNT/PSS/PAH (+32.28 mV) indicates that some free amine groups ($-NH_3^+$) are available for further interaction. The p-CNT/PSS/PAH was further coated with anionic PAA (0.6 mg/mL), and the necklace structure of p-CNT/PSS/PAH/PAA was obtained (Fig. 1d-f and S2). When the PSS was coated onto the p-CNTs, the thickness of PSS at the bumps was approximately 8 nm, which was 4-fold greater than the normal thickness of PSS (approx. 2 nm). This result means that the PSS was coated onto the p-CNTs as the entangled form and led to the formation of bump structures on the p-CNTs. In the case of coating PAH onto the p-CNTs, no bump structures were observed (Fig. S4). We speculate that the PSS possessing benzene ring moieties, which can effectively interact with p-CNTs, is coated as the entangled form as a result of van der Waals interactions, compared to the PAH. Based on the p-CNT/PSS template, we believe that the formation of necklace structures was completed using a nonstoichiometric ratio of PEs (p-CNT/PSS/PAH to PAA). We have previously reported the synthesis of self-assembled spherical polyelectrolyte complexes (PECs) in aqueous solution by controlled mixing of PAH and PAA in a nonstoichiometric ratio.[9] The driving force for the formation of spherical PECs is mainly based on the electrostatic interactions between the carboxylic groups of PAA and amino groups of PAH in a nonstoichiometric ratio. In a similar way, a nonstoichiometric ratio of PAH to PAA was applied for the coating of p-CNT/PSS. We assume that the PSS noncovalently interacted with p-CNT in the bumps on the p-CNT/PSS template through their non-charged parts (benzene groups) and that the active charged groups (sulfonates) exist as the free species. These charged groups in the bumps are available for binding the oppositely charged amino groups of PAH. Subsequently, the PAA is also assembled onto certain irregular bumps. Therefore, neuron-like structures could be formed on the p-CNTs. However, in the case of a stoichiometric ratio of p-CNT/PSS/PAH to PAA, no neuron-like structures were formed and p-CNT/PSS/PAH/PAAs were precipitated (Fig. S5). These

New Journal of Chemistry Accepted Manuscript

results indicate that the neuron-like structures can only be formed or developed by using nonstoichiometric ratios of PAH based on a p-CNT/PSS template.

Studies of metal NPs have recently received substantial interest because of their wide range of potential applications in the biomedical, environmental, and electronic fields. In addition, considerable endeavors have been directed toward covalently or noncovalently attaching metal NPs onto the sidewalls of CNTs and constructing the corresponding multifunctional hybrid nanostructures to achieve a wider range of applications.[21] In this work, the necklace structure of the CNT/PSS/PAH/PAA was employed as a support for loading bi- or tetrametallic NPs, such as Au/Ag, Pt/Ag, Au/Pt, Ag/Pd or Au/Pt/Ag/Pd NPs. For this purpose, metal precursor-loaded PAH (PAH-Au or Pt ions) and PAA (PAA-Ag or Pd ions) were used to assemble the CNT/PSS template instead of bare PAH and PAA (Fig. S6). Controlled loading of metal precursors ensured that 45-50% and 30-43% of the charged groups in the PAH ($-NH_3^+$) and the PAA ($-COO^-$), respectively, were available for further interactions with the oppositely charged groups in subsequent steps, as we reported earlier.[18] Therefore, metal precursor-embedded PAH and PAA also enable the construction of a necklace structure on CNT/PSS. After co-reduction of the multi-metallic precursor-embedded CNT/PSS/PAH/PAA using $NaBH_4$, we obtained the corresponding metal NP-decorated neuron-like structures. Average size of metal NPs embedded in p-CNT/PSS/PAH/PAA and comparative component ratio was depicted in Fig S7-S9.

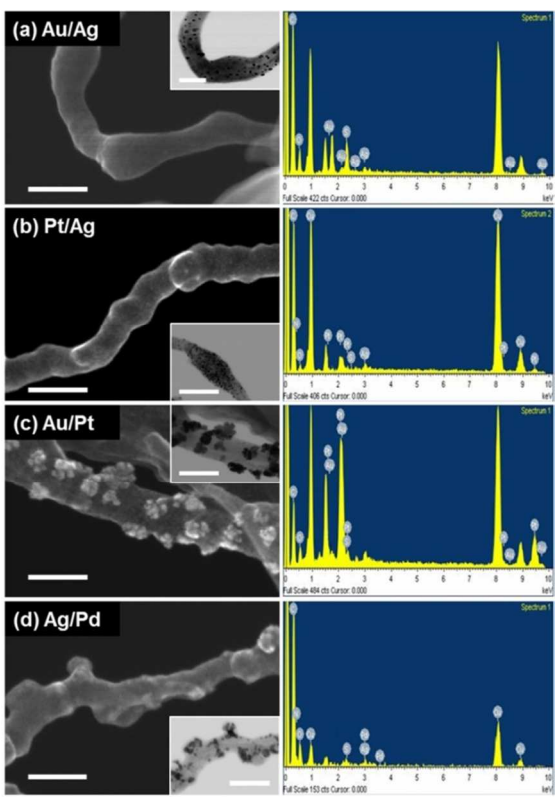

Fig. 3 UHR-FESEM micrographs for bimetallic NP-embedded p-CNT/PSS/PAH/PAA with the corresponding EDX spectra. Insets are the corresponding STEM images. All scale bars represent 50 nm.

Thermal gravimetric analysis (TGA) is generally used for the determination of non-carbon contents such as metal catalysts in CNT.[22] Therefore, TGA was performed to identify the metal contents for all composite materials under an air atmosphere at a heating rate of 5 ^oC/min in temperature range from 30 to 700 °C (Fig. S10). The obtained TGA data show two major weight losses attributed to decomposition of polymer or amorphous carbon (200 ~ 400 ^oC) and CNT itself (400 ~ 600 ^oC). Since p-CNT/PSS/PAH/PAA in the absence of metal NPs was also contained 4% of metal components used as catalysts for CNT growth, the residual metal contents in p-CNT/PSS/PAH/PAA-*M* were calculated by subtracting residual wt% (4.04%) of the bare p-CNT/PSS/PAH/PAA. The calculated wt% of metal component was summarized in Table S1. According to the TGA data, Ag or PdNPs containing bimetallic p-CNT/PSS/PAH/PAA-*M* (*M*=Au/Ag and Ag/Pd) shows higher wt% of metal contents, *i.e.* 33% and 28.8%, respectively compare to that of *M*=Au/Pt (17.9%). This result may come from due to the existence of plenty of anionic sulfonate and carboxylic groups in PSS and PAA, respectively for the binding of cationic metal precursors. In contrast, Au or Pt only can interact with the amino groups of PAH. Tetrametallic one (*M*=Au/Ag/Pt/Pd) contains 38.2 % of metal residue.

The UHR-SEM images show that metal NPs composed of Au/Ag or Pt/Ag are homogeneously distributed on the CNT/PSS/PAH/PAA (Fig. 3a and 3b). However, when the same charges of metal precursors, such as $AuCl_4^-/PtCl_6^{2-}$ or Ag^+/Pd^{2+}, were employed, the distribution of metal NPs on the CNT/PSS/PAH/PAA was slightly different and not homogeneous (Fig. 3c and 3d). It is presumed that charged groups ($-NH_3^+$ or $-COO^-$) are differently allocated (not homogeneous) throughout the CNT/PSS/PAH/PAA because Au/Pt and Ag/Pd NPs are mainly synthesized on amine ($-NH_3^+$) and carboxylic ($-COO^-$) groups, respectively. Therefore, metal ions with the same charges are concentrated on certain points of the CNT/PSS/PAH/PAA. This result indicates that the CNTs were not completely or homogeneously covered with PEs upon each PE coating, which led to the formation of bump structures on the CNTs.

Fig. 4 shows highly loaded tetrametallic NPs on CNT/PSS/PAH/PAA structures, and the EDX data confirm their existence. Four types of NPs were homogeneously distributed throughout the CNT/PSS/PAH/PAA structures due to the use of oppositely charged metal precursors. This result indicates that the proposed necklace structure of CNT/PSS/PAH/PAA could be a promising support for the loading of multi-metallic NPs with ultrahigh density.

It is reported that, the co-reduction method of multi-metallic precursors produces intermetallic or alloy-typed NPs.[8,9] Core/shell and heterostructure NPs are more easily synthesized by seeded-growth strategy.[18] To identify the structure analysis of metal NPs in CNT/PSS/PAH/PAA matrix, X-ray diffraction (XRD) analysis was performed. X-ray diffraction (XRD) pattern of monometallic NP-embedded CNT/PSS/PAH/PAA, where the metal was Au, Ag, Pt and Pd was indexed to (111), (200), (220) and (300) facets of a face-centre-cubic lattice with their corresponding diffraction pattern of (111) planes at 38.30^o, 38.27^o, 38.50^o and 38.51^o, respectively (Fig. S11a). On the other hand, the patterns of the (111) plane of bimetallic NP-CNT/PSS/PAH/PAA were detected at 38.0^o, 38.07^o and 38.1^o for Au/Ag, Ag/Pd and Au/Pt, respectively with lower angle-side shift compare to their individual NPs (Fig. S11b). Generally, as the metallic bond-length of multi-metallic alloy

New Journal of Chemistry Accepted Manuscript

This journal is © The Royal Society of Chemistry 2012

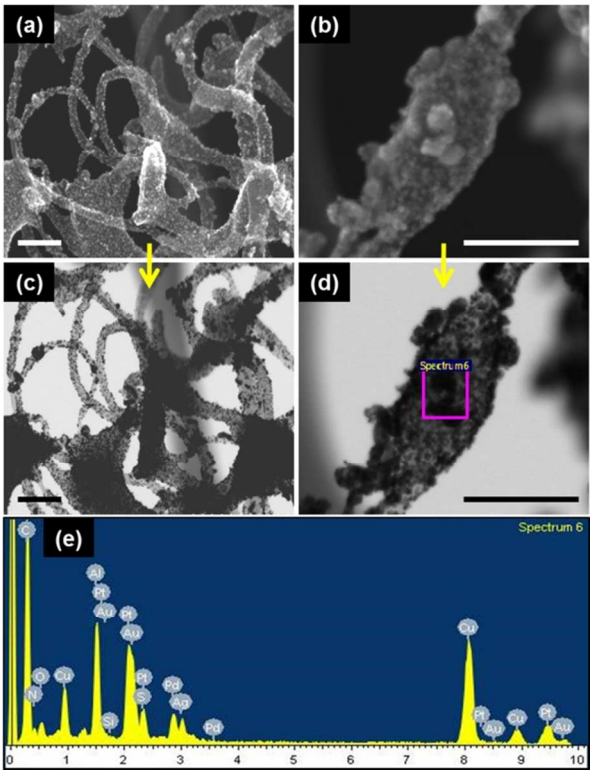

Fig. 4 (a-d) UHR-FESEM micrographs for tetrametallic NP-CNT/PSS/PAH/PAA in (a and c) low and (b and d) high magnification. All scale bars represent 100 nm. (e) Corresponding EDX data. The EDX data confirm the existence of metal NPs (Au/Pt/Ag/Pd).

NPs increases, the spacing between the adjacent planes of NPs also increases in comparison to the spacing obtained before the formation of the alloy.[23,24] The obtained results reveal an expansion of the lattice due to the formation of alloy-typed bimetallic composition. In case of tetrametallic system, p-CNT/PSS/PAH/PAA-*M* (*M*=Au/Pt/Ag/Pd), we also observed a similar tendency with bimetallic system showing a wide-ranged peak at 37.74° which appeared at lower angle position than their constituent metal NPs.

XPS spectra can provide us with further information regarding the chemical state of the alloy NPs and their comparative component ratio in the p-CNT/PSS/PAH/PAA supports. Fig. S12 presents the XPS spectra of bi-, and tertametallic NP-embedded CNT/PSS/PAH/PAA displaying Au/Ag, Au/Pt, Ag/Pd and Au/Ag/Pt/Pd NPs consisted of doublets of each constituent metal particle corresponding to zero-valence (metallic) states of Au, Ag, Pt and Pd.[25-27] Fig. S13 displays deconvoluted XPS data for Ag 3d of AgNPs containing CNT supports, where both Ag $3d_{5/2}$ and Ag $3d_{3/2}$ could be resolved into two peaks, respectively. The peaks for the Ag $3d_{5/2}$ (368.3 ~ 368.4 eV) and Ag $3d_{3/2}$ (374.3 ~ 374.4 eV) could be assigned to metallic Ag (blue dot lines), and the weak peaks for the Ag $3d_{5/2}$ (367.5 eV) and Ag $3d_{3/2}$ (373.8 eV) peaks could be assigned to oxidized Ag (green dot lines).[28] We believe the partially oxidized silver may be due to an exposure to air during reduction process. Table S2 shows the comparative mass% obtained from XPS analysis for each metal component in bi-, and tetrametallic system, which shows almost identical to metal composition ratio (%) observed from EDX analysis (Fig. S8 and S9).

The UV absorbance measurements also conducted to further confirm the synthesis of alloy-typed metal NPs (Fig. S14). For the comparison, mono-, bi-, and tetrametallic compositions were tested. Generally, individual Au and AgNPs exhibit the strong surface plasmon resonance (SPR). The average particle sizes, 9.81 nm for AuNPs and 10.93 nm for AgNPs (Fig. S7) were favourable for obtaining their strong absorbance peaks at 541 and 401 mm, respectively (Fig. S14a). In contrast, Pt and Pd did not show any specific absorption due to their weak SPR effects. In case of bi-, and tetrametallic compositions, broad and single UV absorbance peaks appeared, which seemed to be average of their constituent metal NPs (Fig. S14b). For example, UV absorbance peaks of bimetallic NP-CNT/PSS/PAH/PAA were detected at 483 nm, 515 nm and 387 nm for Au/Ag (Ave. size 5.37 nm), Au/Pt (Ave. size 8.9 nm) and Ag/Pd (Ave. size 5.07 nm), respectively in broaden feature. In addition, the absorption peak of tetrametallic Au/Pt/Ag/Pd became more broaden than that of bimetallic one. These results are clearly different from core-sell or separate entities structure which have been characterized in our previous report[18]. Therefore, it could be confirmed that bi-, or tetrametallic alloys were formed after loading and co-reduction of metal precursors onto the p-CNT/PSS/PAH/PAA surface.

To explore potential applications of the neuron-like structures, bi- and tetrametallic NP-CNT/PSS/PAH/PAA composites were employed as catalysts for the reduction of 4-nitrophenol (4-NPh). As a model system, the reduction of 4-NPh, which is a toxic material generated from industrial wastewater, to 4-aminophenol (4-APh) was chosen. After the addition of the catalysts into a 4-NPh solution, the conversion rates of the reaction were monitored using UV-vis absorption spectroscopy. As the reaction progressed, the absorption peak of 4-NPh at 400 nm slowly diminished with the simultaneous appearance of a new peak at approximately 300 nm in all cases,[29] which indicates the formation of 4-APh (Fig. S15). The conversion rate after 3 minutes for the reduction of 4-NPh to 4-APh using tetrametallic NP-CNT/PSS/PAH/PAA was 96.8%, which was higher than the bimetallic NP-CNT/PSS/PAH/PAA (Fig. 5a and 5b). It was hypothesized that the better performance of the tetrametallic sample resulted from the synergetic effect between multi-metallic NPs and the increasing number of NPs. In general, it is well known that AuNPs have a higher catalytic effect on the reduction of 4-NPh than other noble metal NPs. Therefore, bimetallic catalysts containing Au NPs exhibited a higher rate of conversion than other bimetallic compositions. More interestingly, the conversion rate obtained using the tetrametallic NP-CNT/PSS/PAH/PAA was even higher than that obtained using the tetrametallic NP-polymer particles, in which the metal NPs were prepared using the same method as the current work, as previously reported.[18] We believe that the enhanced catalytic properties are attributed to the CNTs possessing large surface areas and metallic properties, which provide high NP loading and effective electron transport, respectively. For parallel comparison, the p-CNT/PSS/PAH/PAA itself as a matrix was also tested for the catalytic performance. The p-CNT/PSS/PAH/PAA showed extremely lower catalytic property, and the reduction did not complete for more than 1 hour (Fig. S17). It means that without metal NP catalysts in p-CNT/PSS/PAH/PAA matix, the catalytic reaction did not proceed.

New Journal of Chemistry Accepted Manuscript

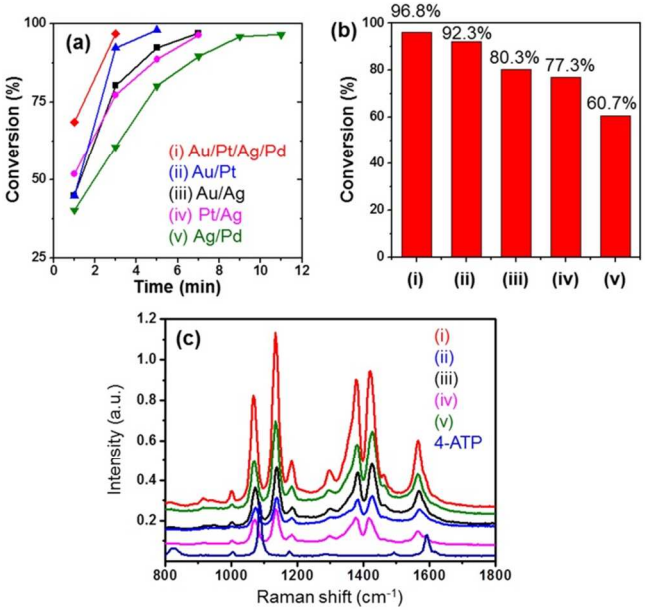

Fig. 5 (a) The conversion rates for the reduction of 4-NPh in the presence of bi- and tetrametallic NP-CNT/PSS/PAH/PAA. (b) Comparative % of conversion after 3 min. (c) SERS spectra of 4-ATP adsorbed on the bi- and tetrametallic NP-CNT/PSS/PAH/PAA.

Furthermore, structural integrity for the reusability for the reduction of 4-NPh has been investigated using the tetrametallic system as a representative catalyst. Fig. S16 shows comparative catalytic performance of p-CNT/PSS/PAH/PAA-*M* (*M*=Au/Ag/Pt/Pd) for the 1st and 2nd uses. Although the reduction rate was relatively slow, it took 7 min to reduce 95% of 4-NPh for the 3rd use, it still showed enough amount of metal catalysts within p-CNT/PSS/PAH/PAA maintaining their similar size with that of before using for further catalytic use. Slightly deformed structure of the p-CNT/PSS/PAH/PAA after the 3rd use might be due to a mechanical stress during the multiple washing processes using centrifugation (15000 rpm for 15 min) for its separation from the mixture (Fig. S16f).

We also evaluated the SERS activities of bi- and tetrametallic NP-CNT/PSS/PAH/PAA for the fabrication of significant SERS substrates. Fig. 5c displays the Raman spectra before and after the adsorption of 4-aminothiophenol (4-ATP) onto the surfaces of the tetrametallic NP- CNT/PSS/PAH/PAA. The respective peak shifts from 1082 cm^{-1} (a_1 vibrational mode) and 1591 cm^{-1} to 1066 cm^{-1} and 1563 cm^{-1} were observed due to the formation of strong chemical bonds by direct contact of the thiol groups in 4-ATP with the metal NPs in the CNT/PSS/PAH/PAA.[30] Other peaks located at 1134, 1180, 1377, 1419 and 1563 cm^{-1} (b_2 vibrational modes) became stronger compared to those of bare 4-ATP. A significant charge transfer (CT) contribution was shown by the considerable enhancement of b_2 at 1134 cm^{-1} compared to that of a_1 at 1066 cm^{-1}. For tetrametallic NP (Au/Pt/Ag/Pd), bimetallic NP (Ag/Pd), and bimetallic NPs (Au/Ag), the relative intensity ratios of b_2/a_1 were 1.48, 1.32, and 1.15, respectively. In addition, the comparative intensity ratios, such as $I_{1134(Au/Pt/Ag/Pd)}/I_{1134(Ag/Pd)}$ and $I_{1134(Au/Pt/Ag/Pd)}/I_{1134(Au/Ag)}$, were 1.72 and 2.51, respectively. These results suggest that tetrametallic NP-CNT/PSS/PAH/PAA has a higher rate of charge transfer between metal NPs and the 4-ATP molecules compared to that of bimetallic compositions. For the tetrametallic composition, the interstitial gaps present between the adjacent metallic nanostructures reduced due the increasing number of NPs, and the coupled plasmon resonance shifted to the red. Therefore, the electromagnetic field increases at the junction of the aggregated NPs, called the 'hot spots', upon optical excitation. The hot spots are greatly favorable for enhancing SERS effects.[31] Moreover, the high aggregation tendency of Ag may contribute to producing a large number of electromagnetic hot spots.[32] For this reason, CNTs containing AgNPs, such as CNT/PSS/PAH/PAA-Au/Ag or -Ag/Pd, showed higher SERS effects than CNTs without AgNPs.

IV Conclusions

In conclusion, neuron-like structures consisting of CNTs and PEs were successfully prepared and utilized for the ultrahigh loading of multi-metallic NPs. The CNTs coated with PSS were used as a template for the neuron-like architecture using the sequential adsorption of PAH and PAA in a nonstoichiometric ratio. Because the PSS formed discontinuous bumps on the surface of the CNTs, successive PAH and PAA were assembled onto the irregular bumps on the CNT/PSS, which led to the formation of neuron-shaped hybrid structures. The self-assembly of PEs on CNTs yields neuron-like structures, which provide increased surface area and binding sites for a high loading of multi-metallic NPs. Moreover, it exhibited a selective binding tendency and special arrangement of NPs when the same types of metal precursors were used, which indicates that the distribution of certain types of NPs can be controlled within the nanostructures. The multi-metallic NP-embedded CNT/PSS/PAH/PAA was demonstrated to be a SERS substrate and catalyst for the reduction of 4-NPh. We expect that the methodology presented here can be extended to other systems, opening up novel applications through the synthesis of unique nanostructures.

Acknowledgements

This work was supported by the Korea Basic Science Institute (KBSI) grant T34740 and a grant from the cooperative R&D program funded by the Korea Research Council for Industrial Science and Technology.

Notes and references

[a]Western Seoul Center, Korea Basic Science Institute, 150 Bugahyunro, Seodaemun-gu, 120-140, Seoul, Republic of Korea
E-mail:hajinlee@kbsi.re.kr
[b]Department of Chemical and Biological Engineering, Hanbat National University, 125 Dongseodaero, Yuseong-gu, 305-719, Daejeon, Republic of Korea
E-mail: choiws@hanbat.ac.kr

Electronic Supplementary Information (ESI) available: Zeta potential data and TEM and SEM images, including EDX, of PE-coated CNTs; XPS data for the characterization of CNT/PSS/PAH and CNT/PSS/PAH/PAA; synthesis scheme for multi-metallic NP-CNT/PSS/PAH/PAA; UV-vis absorption data for the comparative catalytic abilities of multi-metallic NP-CNT/PSS/PAH/PAA.. See DOI: 10.1039/b000000x/

New Journal of Chemistry Accepted Manuscript

This journal is © The Royal Society of Chemistry 2012

1. K. Gong, D. Su and R. R. Adzic, *J. Am. Chem. Soc.* 2010, **132**, 14364.
2 S. Ikegami and H. Hamamoto, *Chem. Rev.* 2009, **109**, 583.
3 D. Astruc, F. Lu and J. R. Aranzaes, *Angew. Chem. Int. Ed.* 2005, **44**, 7852.
4 R. Akiyama and S. Kobayashi, *Chem. Rev.* 2009, **109**, 594.
5 B. H. Ong, X. C. Yuan and S. C. Tjin, *Fiber Integr. Opt.* 2007, **26**, 229.
6 X. K. Liu, B. Y. Dai, L. Zhou and J. Q. Sun, *J. Mater. Chem.* 2009, **19**, 497.
7 M. Dierendonck, S. D. Koker, R. De Rycke, P. Bogaert, J. Grooten, C. Vervaet, J. P. Remon and B. De Geest, *ACS Nano* 2011, **5**, 6886.
8 Md. A. Rahim, B. Nam, W.S. Choi, H.-J. Lee and I. C. Jeon, *J. Mater. Chem.*, 2011, **21**, 11831.
9 Md. S. Islam, W. S. Choi, H.-J. Lee, Y. B. Lee and I. C. Jeon, *J. Mater. Chem*., 2012, **22**, 8215.
10 Md. A. Rahim, Md. S. Islam, T. S. Bae, W. S. Choi, Y. Y. Noh and H.-J. Lee, *Langmuir* 2012, **28**, 8486.
11 L. Zhang, M. Zheng, X. Liu and J. Q. Sun, *Langmuir* 2011, **27**, 1346.
12 T. C. Wang, M. F. Rubner and R. E. Cohen, *Langmuir*, 2002, **18**, 3370.
13 L. Qu, R. A. Vaia and L. Dai, *ACS Nano* 2011, **5**, 994.
14 M. Michel, A. Taylor, R. Sekol, P. Podsiadlo, P. Ho, N. Kotov and L. Thompson, *Adv. Mater.* 2007, **19**, 3859.
15 M. N. Zhang, Y. M. Yan, K. P. Gong, L. Q. Mao, Z. X. Guo and Y. Chen, *Langmuir* 2004, **20**, 8781.
16 M. N. Zhang, L. Su and L. Q. Mao, *Carbon* 2006, **44**, 276.
17 S. E. Moya, A. Ilie, J. S. Bendall, J. L. Hernandez-Lopez, J. Ruiz-García and W. T. S. Huck, *Macromol. Chem. Phys*. 2007, **208**, 603.
18 Md. S. Islam, W. S. Choi, Y. B. Lee and H.-J. Lee, *J. Mater. Chem. A* 2013, **1**, 3565.
19 S. H. Lee, J. S. Park, B.K. Lim and S. O. Kim, *J. Appl. Polym. Sci.* 2008, **110**, 2345.
20 F. Li, Z. Wang, C. Shan, J. Song, D. Han and L. Niua, *Biosens. Bioelectron*. 2009, **24**, 1765.
21 W. Yang, X. Wang, F. Yang, C. Yang and X. Yang, Adv. *Mater*. 2008, **20**, 2579.
22 J. H. Han, K. H. An, N. S. Lee, J. C. Goak, M. S. Jeong, Y. C. Choi, K. H. Oh, K. K. Kim and Y. H. Lee, *Carbon Lett.* 2009,**10**, 5.
23 B. A. Kakade, T. Tamaki, H. Ohashi, and T. Yamaguchi. *J. Phys. Chem. C* 2012, **116**, 7464.
24 S. Alayoglu, P. Zavalij, B. Eichhorn, Q. Wang, A. I. Frenkel, and P. Chupas. *ACS NANO* 2009, **3**, 3127.
25 J. Yang, E. H. Sargent, S. O. Kelley and J. Y. Ying, *Nature Mat.*2009, **8**, 683.
26 N. Ilayaraja, N. Prabu, N. Lakshminarasimhan, P. Murugan and D. Jeyakumar, *J. Mater. Chem. A* 2013, **1**, 4048.
27 A.-Q. Wang, J.–H. Liu, S.D. Lin, T.-S. Lin and C.–Y. Mou, *J. Catal.* 2005, **233**, 186.
28 L. Shang, L. Jin, S. Guo, J. Zhai and S. Dong, *Langmuir* 2010, **26**, 6713.
29 S. K. Ghosh, M. Mandal, S. Kundu, S. Nath and T. Pal, *Appl. Catal. A* 2004, **268**, 61.
30 G. Wei, L. Wang, Z. Liu, Y. Song, L. Sun, T. Yang and Z. Li, *J. Phys. Chem. B*, 2005, **109**, 23941.
31 T. Wang, X. Hu and S. Dong, *Small* 2008, **4**, 781.
32 G. C. Schatz, *Acc. Chem. Res*. 1984, **17**, 370.

New Journal of Chemistry Accepted Manuscript